

PREDICTION OF TURBOMACHINERY AEROELASTIC BEHAVIOR FROM A SET OF REPRESENTATIVE MODES

María A. Mayorca

Royal Institute of Technology
Heat and Power Technology
S-100 44 Stockholm, Sweden

Damian M. Vogt

Royal Institute of Technology
Heat and Power Technology
S-100 44 Stockholm, Sweden

Hans Mårtensson

VOLVO Aero Corporation
S-461 81 Trollhättan, Sweden

Torsten H. Fransson

Royal Institute of Technology
Heat and Power Technology
S-100 44 Stockholm, Sweden

ABSTRACT

A method is proposed for the determination of the aeroelastic behavior of a system responding to mode-shapes different to the tuned in-vacuo ones, due to mistuning, mode family interaction or any other source of mode-shape perturbation. The method is based on the generation of a data base of unsteady aerodynamic forces arising from the motion of arbitrary modes and uses Least Square approximations for the prediction of any responding mode. The use of a reduced order technique allows for mistuning analyses and is also applied for the selection of a limited number of arbitrary modes. The application on a transonic compressor blade shows that the method captures well the aeroelastic properties in a wide frequency range. A discussion of the influence of the mode-shapes and frequency on the final stability response is also provided.

1 INTRODUCTION

In turbomachinery the vibration of the blades leads to fluid pressure unsteadiness which can 1) attenuate the vibration of the blades in which case it is referred as a positive aerodynamic damping and is an important contributor on the forced response or 2) lead to a rapidly increasing vibration amplitude in an unstable self-excited condition which is known as flutter, and needs to be avoided in the operating range of the machine. In the context of this paper aeroelastic behavior refers to both of these phenomena.

It is a common practice to predict the aeroelastic behavior (or stability) of a system by performing unsteady Computational Fluid Dynamics (CFD) calculations. As first approach, the stability of the first three pure modes of the blade are usually considered at different relevant operating points, giving an indication if the blade design is acceptable with respect to the flutter margins. This is usually assessed

by using an analogue mass spring system including the unsteady aerodynamics as contributors on the stiffness and the damping [1]. The same concept has been considered by the Fundamental Mistuning Model (FMM) [2-3] and the Asymptotic Mistuning Model (AMM) [4-5] for studying the effect of both structural and aerodynamic mistuning on the aeroelastic behavior of turbomachinery, both in forced response and aerodynamic damping analyses. These methods have the great advantage of being very efficient with respect to computational time since generalized coordinates (instead of the full structural meshes) are considered for analyzing individual mode families. However, these approaches are most suitable when no interaction between the mode families is present, or when the mode-shapes of the blades are fairly similar to the original tuned in-vacuo case. Previous studies [6-7] have shown that when two blade mode families interact (e.g. bending and torsion interaction), the aerodynamic damping predicted can be of considerable difference as for the one predicted for a single mode family. Turbomachinery design is today more and more pushing towards lighter and twisted blades and exposed to larger aerodynamic loads (e.g. open rotors) which imply a reduction of the mass ratio in favor of the possibility of mode family interaction. Clark et al. [8] proposed a methodology for determining when a possibility of mode interaction flutter is present. This method determines a critical mass ratio below which flutter can occur as a function of the frequency and solidity of the blade.

A method for considering mistuning as well as mode family interaction was presented by Mayorca et al. [9] and is referred to as the Multimode Least Square (MLS) model. The method includes in the dynamic equation of motion the different unsteady aerodynamic damping forces rising from

the oscillation of mode-shapes of interest. This is done by fitting the unsteady aerodynamic influences from the different modes-shapes in a single aerodynamic stiffness and a single damping matrix by Least Square (L^2) approximations. This approximation is based on the linear behavior of the unsteady forces with respect to the mode-shape in the region of small amplitudes as demonstrated both numerically and experimentally by Glodic et al. [10].

The MLS was applied in a transonic compressor blade, and it was observed how mistuning could cause veerings between two mode families and consequently changing the aerodynamic damping behavior of the system. For that application, the mode interaction behavior was obtained from the unsteady forces of the known in-vacuo modes.

In the present study, the MLS method is applied in a more general manner, by determining aerodynamic matrices from a set of unsteady forces produced from the oscillation of arbitrary modes. In this sense, the aeroelastic properties of the system dynamic equation of motion is not restricted to only the in-vacuo modes but also to a system responding to perturbed modes. The main reason for developing this model is to be able to account for sources that lead to changes of the in-vacuo modes-shapes, such as: mistuning, coating damping, mode family coupling, a large impact from aerodynamic forces (largely damped blades), cracks, dampers, inter-shroud connectivity or other sources of mode-shape perturbations, as long as the steady aerodynamics are preserved constant.

The present paper aims at establishing a procedure for selecting an optimum set of arbitrary mode-shapes (referred as Guyan-based Arbitrary Modes, GAMs) that can be used for the prediction of aeroelastic behavior of a perturbed system in a wide general sense. It also gives an estimation of how accurate the method could be with respect to the computational effort.

There are two main challenges in this process: 1) the selection of relevant arbitrary modes that keep accuracy and computational efficiency inside reasonable margins; 2) including the frequency content in the system from forces obtained having oscillated GAMs which do not have an associated eigen-frequency.

Challenge 1 is here assessed by the use of a standardized reduction technique proposed by Guyan [12] which allows reducing the size of the dynamic system to selected master nodes. The Guyan reduction concept is also used for producing different sets of arbitrary modes, as it is explained in this paper. Accuracy is evaluated in terms of how well the arbitrary mode-shapes fit to the first in-vacuo mode-shapes and to their resulting aeroelastic behavior. Challenge 2 is overcome by the calculation of different sets of unsteady forces from the arbitrary modes oscillated at the extreme values of the frequency range of interest, and evaluating what would be the limits at which the forces can be fitted accurately. A similar approach was presented by Mårtensson [11] in a wing profile. It was shown that the frequency effect could be included in the dynamic system by fitting the real part of the forces from a mode oscillated at two frequencies to the aerodynamic mass and stiffness. However, the imaginary part of the forces can only be fitted linearly to only one frequency.

The paper is divided in the following sections: first a description of the Multimode Least Square method (MLS) and its general application is given followed by the description of the method considering arbitrary modes. Then the reduction technique implemented for reducing the model size is assessed. The application of the method is performed on a highly loaded transonic compressor blade where a general procedure for selecting the arbitrary modes (GAMs) and its final accuracy with respect to the reference case is evaluated. Finally, the influence of the frequency and the mode-shapes in the final aeroelastic behavior is discussed.

2 NOMENCLATURE

A_{\max}	Mode maximum amplitude, [mm]
a	Generalized Coordinate [-]
C	Damping matrix [Ns/m]
\hat{C}_p	Unsteady pressure coefficient: $\hat{C}_p = \frac{\hat{p}}{(p_o - p) \cdot A_{\max}}, [\frac{1}{mm}]$
dof	Degree of freedoms: X, Y, Z
F	Force vector [N]
f	frequency, [Hz]
G	Matrix of modal forces [N]
H	Matrix of modal forces divided by the frequency of oscillation [Ns/rad]
K	Stiffness matrix [N/m]
M	Mass matrix [Kg]
m	Number of modes [-]
P	Pressure, [Pa]
P	Modal displacement vector [m] Modal displacement matrix [m]
q	Back-expanded mode vector, [m]
t	Time [s]
X	Cartesian coordinate. In this context represent the axial direction, [-]
x	Displacement vector [m]
Y	Cartesian coordinate. In this context represents the radial direction, [-]
y	Approximation to the displacement vector x [m]
Z	Cartesian coordinate. In this context represents the tangential direction, [-]
Symbols	
ω	Frequency [rad/s]
ϕ	Modal vector, [-]
L^2	Least Square
Re	Real part of the complex number, [-]
Im	Imaginary part of the complex number, [-]
Superscript	
k	Node number, referred to the stiffness matrix
c	Referred to the damping matrix
T	Transpose
-1	Inverse
\wedge	Complex
\dots	First and second derivative
Subscript	

AERO	Refers to the system aerodynamic block circulant matrix
aero	Refers to the influence coefficient Aerodynamic matrix
G	Guyan reduced Generalized
g	Generalized
INFC	Influence Coefficient
i	Vibration mode index
n	Maximum number of GAMs
m	Master nodes
max	Maximum
min	Minimum
mean	Mean value
o	Referent to total quantities
perturbed	Refers to the responding perturbed mode
s	Slave nodes
STRU	Refers to the system structural matrix
Abbreviations	
AROMA	Aeroelastic Reduced Order Modeling Analysis
CFD	Computational Fluid Dynamics
GAM	Guyan-based Arbitrary Mode
IBPA	Inter Blade Phase Angle
INFC	Influence Coefficient
FE	Finite Element
MAC	Modal Assurance Criteria
MLS	Multimode Least Square
PS	Pressure Side
SCA	Stability Curve Amplitude
SDOF	Single Degree of Freedom
SS	Suction Side
TWM	Travelling Wave Mode

3 APPROACH

3.1. MLS General Method

A detailed description of the MLS method is given in [10] and the main concept is summarized here for the sake of completeness. Its application in stability analyses is discussed in this paper, and thus consideration of forces only produced due to blade motion are included.

The method considers the homogenous solution of the dynamic equation of motion, considering unsteady forces rising from blade vibration of different modes as aerodynamic matrices, as presented in the set of equations 1.

$$\begin{aligned}
M \cdot \ddot{X}(t) + C \cdot \dot{X}(t) + K \cdot X(t) &= 0 \\
X(t) &= \hat{x} \cdot e^{i\omega t} \\
\dot{X}(t) &= i \cdot \omega \cdot \hat{x} \cdot e^{i\omega t} \\
\ddot{X}(t) &= -\omega^2 \cdot \hat{x} \cdot e^{i\omega t} \\
(-\omega^2 \cdot M + i \cdot \omega \cdot C + K) \cdot \hat{x} \cdot e^{i\omega t} &= 0 \\
-\omega^2 (M_{STRU} + M_{AERO}) + i\omega(C_{STRU} + C_{AERO}) + (K_{STRU} + K_{AERO}) &= 0
\end{aligned} \tag{1}$$

K_{STRU} and M_{STRU} are block diagonal matrices containing the structural stiffness and mass of the blade and C_{STRU} consider mechanical damping, mainly rising from material or friction damping. The complex aerodynamic damping forces can be decomposed in the Influence Coefficient domain (INFC) which represents the individual influences of the motion of one blade into another. The complex forces in the INFC domain can then be included in the dynamic system as

contributors proportional to aerodynamic mass, stiffness and damping matrices. The determination of the influence coefficient aerodynamic matrices is assessed by an analogue representation of the dynamic system, but only considering the aerodynamic contributions as shown in equation 2.

$$[-\omega^2 \cdot M_{aero} + i \cdot \omega \cdot C_{aero} + K_{aero}] \{\hat{X}\} = \{\hat{F}_{aero}\} \tag{2}$$

$$\omega \cdot [C_{aero}] \{\text{Im}(\hat{X})\} = \{\text{Im}(\hat{F}_{aero})\} \tag{3}$$

$$[-\omega^2 \cdot M_{aero} + K_{aero}] \{\text{Re}(\hat{X})\} = \{\text{Re}(\hat{F}_{aero})\} \tag{4}$$

The imaginary part of the forces contributes to the aerodynamic damping (C_{aero} , equation 3) and the real part of the forces to the aerodynamic stiffness (K_{aero}) and mass (M_{aero}) as presented in equation 4. It can be assumed that the influence of the aerodynamic mass is small as compared to the aerodynamic stiffness, and thus concentrate all the real force influences in the aerodynamic stiffness term (equations 5 and 6), similar to as applied in single degree of freedom (SDOF) approaches [2-3].

$$[K_{aero}] \{\text{Re}(\hat{X})\} = \{\text{Re}(\hat{F}_{aero})\} \tag{5}$$

$$[C_{aero}] \{\text{Im}(\hat{X})\} = \left\{ \frac{\text{Im}(\hat{F}_{aero})}{\omega} \right\} \tag{6}$$

In the MLS method, the blades are not considered in generalized coordinates, but rather the complete blade FE mesh. Consequently, the solution is not restricted to a single family of modes. Determination of the aerodynamic matrices from the unsteady forces rising from different modes is performed by using Least Square (L^2) approximations.

The mode-shapes of interest, in general a set of in-vacuo modes calculated by Finite Element methods, are used to perform different blade motion CFD unsteady calculations. Since modal displacement vectors (P_i) are used, then

complex modal forces (\hat{G}_i) are obtained for each mode i .

The displacement x of each node k can be approximated to a solution y as a combination of the different m modes proportional to generalized coordinates a as presented in equation 7 and in matrix form in equation 8. Matrix P contains the modal displacement vectors considered in the form $[\{P_1\}\{P_2\} \dots \{P_m\}]$.

$$x^k \approx \sum_{i=1}^m a_i P_i^k = y^k \tag{7}$$

$$\{X\} \approx [P] \{a\} \tag{8}$$

The superscripts refer to the node numbers and the subscripts to the mode number. The exact solution will then be obtained if infinite modes were included. The set of y that approximates best to x can be found by the minimum error for the L^2 , as shown in equation 9 and 10.

$$L^2 = \sum_{k=1}^N \left(\sum_{i=1}^m a_i P_i^k - x^k \right)^2 \tag{9}$$

$$\frac{\partial L^2}{\partial a_i} = 0 \tag{10}$$

After the derivation, the best fit of generalized coordinates is given by equation (11).

$$\{a\} = [P_i^T P_j]^{-1} [P]^T \{x\} \quad (11)$$

Equations 5 and 6 can be written in terms of the modal forces and modal displacement vectors, allowing the aerodynamic matrices to be deduced (equation 12 and 13).

$$\begin{aligned} [K_{aero}] \{Re(\hat{X})\} &= [Re(\hat{G})] [P_i^T P_j]^{-1} [P]^T \{Re(\hat{X})\} \\ [K_{aero}] &= [Re(\hat{G})] [P_i^T P_j]^{-1} [P]^T \end{aligned} \quad (12)$$

$$\begin{aligned} [C_{aero}] \{Im(\hat{X})\} &= [Im(\hat{H})] [P_i^T P_j]^{-1} [P]^T \{Im(\hat{X})\} \\ [C_{aero}] &= [Im(\hat{H})] [P_i^T P_j]^{-1} [P]^T \end{aligned} \quad (13)$$

Matrix $Re(\hat{G})$ contains the real modal force vectors in the form $\{G_1\} \{G_2\} \dots \{G_m\}$ and $Im(\hat{H})$ the imaginary modal forces divided by the frequency at which each mode was oscillated: $\left[\begin{array}{c} \{G_1\} \\ \{G_2\} \\ \dots \\ \{G_m\} \end{array} \right] \left[\begin{array}{c} \omega_1 \\ \omega_2 \\ \dots \\ \omega_m \end{array} \right]$.

The solution of the complete dynamic system (equation 1) will be a perfect match when responding to the frequencies of the mode-shapes included in the P , \hat{G} and \hat{H} matrices. The solution will be fitted by Least Squares for responding modes in a frequency different to that of the modes included in the determination of the aerodynamic matrices. This would be the case when there is a combined mode situation or mode-family interaction.

3.2. MLS Considering Arbitrary Modes

In the MLS general method description, the in-vacuo modes are oscillated in the CFD calculations, and thus both mode-shapes and frequency content is included when determining the aerodynamic damping matrices ($Im(\hat{H})$ in equation 13). In the new application of the method, arbitrary mode-shapes (GAMs) are used instead. As a first condition, they should be linearly independent; and second they should result in an accurate match to any responding perturbed mode-shape (or mode-shapes) when linearly combined, as shown in equation 14. The coefficients a are then determined from L^2 approximations in order to obtain the best possible fit. The responding mode-shape(s) could be in principle any in-vacuo mode or perturbed mode (e.g. a mistuned mode).

$$\{\phi_{perturbed}\} = a_1 \{\phi_{GAM,1}\} + a_2 \{\phi_{GAM,2}\} + \dots + a_n \{\phi_{GAM,n}\} \quad (14)$$

Once the set of arbitrary mode-shapes follow these conditions, it is necessary to select at which frequency (or frequencies) the corresponding modal forces should be determined in the CFD calculations. The selection of the frequency depends on 1) which is the frequency range of interest for the stability analysis and 2) if in that range it is possible to fit in the system both real and imaginary force contributions.

If the frequency range of interest is $[\omega_1 - \omega_2]$, then a first set of aerodynamic forces \hat{F}_{AERO,ω_1} rising from the oscillation of the arbitrary modes at ω_1 is obtained and a second set \hat{F}_{AERO,ω_2} at ω_2 . The two frequency influences could be fitted to the real contributions by determination of the aerodynamic mass and stiffness and solving the system of equations (15). However, the aerodynamic damping matrix can only be approximated by one frequency. If the aerodynamic damping forces major influences behave linearly inside the frequency range, then the aerodynamic damping matrix determined from the set of forces at ω_1 would give a similar result as if it is determined from the set of forces at ω_2 (equation 16).

$$\begin{aligned} [-\omega_1^2 M_{AERO} + K_{AERO}] \{Re(\hat{X})\} &= \{Re(\hat{F}_{AERO,\omega_1})\} \\ [-\omega_2^2 M_{AERO} + K_{AERO}] \{Re(\hat{X})\} &= \{Re(\hat{F}_{AERO,\omega_2})\} \end{aligned} \quad (15)$$

$$\begin{aligned} [C_{AERO,\omega_1}] \{Im(\hat{X})\} &= \left\{ \frac{Im(\hat{F}_{AERO,\omega_1})}{\omega_1} \right\} \\ [C_{AERO,\omega_2}] \{Im(\hat{X})\} &= \left\{ \frac{Im(\hat{F}_{AERO,\omega_2})}{\omega_2} \right\} \end{aligned} \quad (16)$$

After derivation of the L_2 procedure analogue to section 3.1, the aerodynamic mass and stiffness considering the frequency fit and the GAMs can be calculated using equations 17. The aerodynamic damping matrices could be fitted to either extreme frequency (ω_1 or ω_2), or to a mean value of the two, as presented in equation 18.

$$\begin{aligned} M_{aero} &= \frac{[Re(\hat{G}_{aero,\omega_2}) - Re(\hat{G}_{aero,\omega_1})] [P_i^T P_j] [P]^T}{\omega_1^2 - \omega_2^2} \\ K_{aero} &= [Re(\hat{G}_{aero,\omega_2})] [P_i^T P_j] + \omega_2^2 [M_{aero}] \end{aligned} \quad (17)$$

$$\begin{aligned} [C_{aero,\omega_1}] &= [Im(\hat{H}_{\omega_1})] [P_i^T P_j]^{-1} [P]^T \\ [C_{aero,\omega_2}] &= [Im(\hat{H}_{\omega_2})] [P_i^T P_j]^{-1} [P]^T \\ [C_{mean}] &= \frac{[C_{aero,\omega_1}] + [C_{aero,\omega_2}]}{2} \end{aligned} \quad (18)$$

Note that the aerodynamic mass, stiffness and damping matrices obtained in 17 and 18 are representing one influence. This means there are many aerodynamic matrices as influence coefficients. The INFC aerodynamic matrices are then assembled in the overall aerodynamic matrix in the dynamic equation. Specific information on how the system is assembled is given in [10].

3.3. Guyan Reduction

The dynamic system model arising from the MLS method can become very large, since it considers the complete structural FE mesh. The size of the model will depend on the number of blades considered and the number of nodes in the mesh. Note also that the aerodynamic matrices are of circulant nature, being fully populated, and increasing the computational effort. If additionally the disk is incorporated for aerodynamically and structurally coupled analyses, then

the size would be even larger. Even though the formulation of the method allows for aerodynamic and structural mistuning by perturbing the structural properties and aerodynamic influences, its practical application can only be possible by reducing the model size.

For this reason the static condensation technique proposed by Guyan [11] is implemented, which allows reducing to model size to specific selected master nodes by means of static constrained equations. This means that the solution is exact for static problems and is an approximation for dynamic systems. The reduced structural matrices are obtained from the full matrices considering master (or retained) and slaves (or removed) nodes according to equations 19-21. The reduction technique is accurate for the low frequency modes for a reasonable number retained DOF (<2kHz) but still gives an acceptable accuracy as frequency increases.

The Guyan projection can be applied in a rather simple manner depending only on the structural matrices. It also allows for high level structural mistuning and thus is suitable for the current application.

$$K_G = K_{mm} - K_{ms}K_{ss}^{-1}K_{sm} \quad (19)$$

$$(20)$$

$$M_G = M_{mm} - K_{ms}K_{ss}^{-1}M_{ss}K_{ss}^{-1}K_{sm} - K_{ms}K_{ss}^{-1}M_{sm} - M_{ms}K_{ss}^{-1}K_{sm}$$

$$F_G = F_m - K_{ms}K_{ss}^{-1}F_s \quad (21)$$

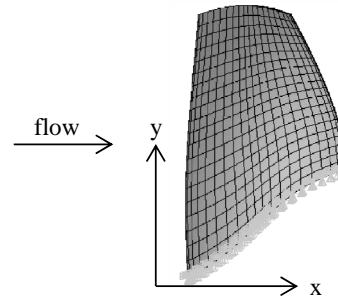
The aerodynamic modal forces are reduced by considering the transformation matrices obtained from the structural stiffness matrices (equation 19). This assumption is valid considering that the structural stiffness is of much larger magnitude than the aerodynamic stiffness. The reduced aerodynamic stiffness and damping are then calculated from the reduced modal displacement and reduced modal force vectors. The final size of the matrices in the model will be $(m \times nb) \times (m \times nb)$, where m is the number of master nodes and nb is the number of blades in the full annulus.

4 APPLICATION

The application of the MLS considering arbitrary modes (GAMs) will be performed on the rotor blade part of a 1 1/2 highly loaded transonic compressor stage [13]. The blade is part of blisk and thus only aerodynamic damping will be considered.

4.1. Finite Element Model

The structural blade mesh is obtained using a Finite Element commercial tool (ANSYS 11.0) and contains a total of 2205 nodes using brick elements of the type Solid 45. The disk is not included in this analysis, having constrained the blade in the hub region (Figure 4-1). Consequently the only coupling between the blades is aerodynamic. The modal analysis of a full single blade mesh is performed considering the pre-stress conditions, such as to include the influence of the mean flow pressure and centrifugal forces effects.



Rotor blade

Figure 4-1: Structural rotor blade mesh



Mode	1	2	3	4	5	6	7
[Hz]	804	1934	2144	3295	3754	4308	4960
Range	f_1						f_7

Table 4-1: First 7 real modes and frequencies. Frequency range considered $[f_1, f_7]$

The frequencies of the first 7 in-vacuo mode-shapes are obtained, and shown in Table 4-1. The frequency range of interest for further analyses is spanned by the f_1 and f_7 .

4.2. CFD Model

The CFD unsteady calculations have been carried out by using the in-house 3D Navier Stokes Linearized code Volsol [14]. The steady state solution was obtained including both rotor and stator domains, and only the solution of the rotor part was considered as bases for the linearized unsteady calculations (Figure 4-2). The operating point considered is at design conditions: 21000 rpm and 2.1 pressure ratio (Figure 4-3).

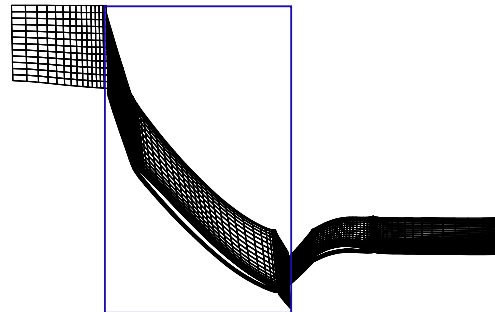


Figure 4-2: Steady state mesh domain. Linearized mesh domain highlighted

The Travelling Wave Mode (TWM) approach is applied for the unsteady calculations, and thus only a single blade passage is computed. For every mode-shape 8 IBPAs are evaluated. A converged solution was considered when the stability curves remained unchanged after two consecutive solutions. The CFD harmonic forces are mapped onto the structural mesh and Fourier transformed in order to obtain the different blade influences according to the influence coefficient approach. The MLS code is built in the numerical tool for aeromechanical analyses AROMA (Aeroelastic Reduced Order Modeling Analysis) [15].

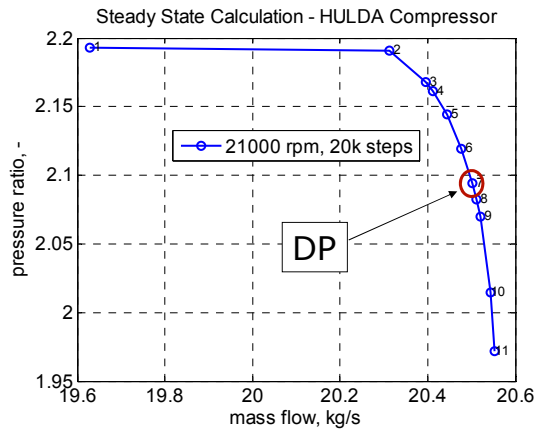


Figure 4-3: 100% speed-line. Design point highlighted

4.3. Analyses Layout

Stability analyses of only aerodynamically coupled blades are considered. The frequency range of interest considers the frequencies from the 1st until the 7th in-vacuo modes. This range is consistent with the Guyan reduction limits of accuracy, but yet is a large enough range of frequency variation keeping in mind the general application of the method. The set of master nodes is selected such as to achieve a good accuracy in mode-shape as well as in frequency with respect to the full blade mesh model. A procedure for the selection of the arbitrary modes based on the Guyan reduction is given, and discussed in a specific section. The reference case is the resulting stability of the first 7 in-vacuo mode-shapes from the MLS general method which will be compared with the following analyses:

- 1) The resulting stability considering the harmonic forces from the arbitrary modes oscillated at f_1 . Only aerodynamic stiffness and damping matrices considered
- 2) The resulting stability from the arbitrary modes oscillated at the frequency f_7 . Only aerodynamic stiffness and damping matrices considered.
- 3) The resulting stability from the arbitrary modes oscillated at frequency f_4 . Only aerodynamic stiffness and damping matrices considered.
- 4) The resulting stability from the arbitrary modes oscillated at 1) frequencies f_1 and f_4 and 2) frequencies f_4 and f_7 . Here both the aerodynamic mass and stiffness matrices are included. The aerodynamic damping matrix is calculated from the average of the resulting aerodynamic matrices determined from the extreme frequencies in each of the ranges.

In order to understand the frequency effect further, the computation of the 1st in-vacuo mode is performed at the 7 different frequencies inside the studied range. Finally a discussion considering the distributed unsteady pressures in relation to the mode-shapes as well as to the steady state pressure field is presented.

5 ARBITRARY MODES SELECTION

The main condition for selecting the arbitrary modes is that they should be linearly independent and when linearly

combined, they should result in a good approximation of any given mode. The ideal case would be to produce a mode in each Cartesian direction for each node of the blade mesh. This means oscillating each node independently at the different IBPAs which in turn will produce a large data base of aerodynamic damping forces that could superpose linearly and give rise to any possible vibration shape. Doing this would require an enormous amount of CFD calculations (e.g. 2205nodes x 3dof x 8 ibpa at f_1 and/or f_7). With the aim of considering a limited number of arbitrary representative modes it is proposed using the Guyan projection concept as the bases of the arbitrary modes generation. In this manner, the amount of arbitrary modes is consistent with the master nodes selected for the structural reduced model and the CFD required calculations can be reduced to a considerably minimum. In the following sections the description of the master node selections and its further use for the arbitrary modes generation is presented.

5.1. Master Nodes Selection

The selection of master nodes has been performed in order to fit accurately the first 7 real mode shapes in the frequency range of interest. The initial set of master nodes was selected considering the following: 1) they should cover locations of expected high energy, 2) master nodes should not be placed too close to each other such as to avoid redundancy.

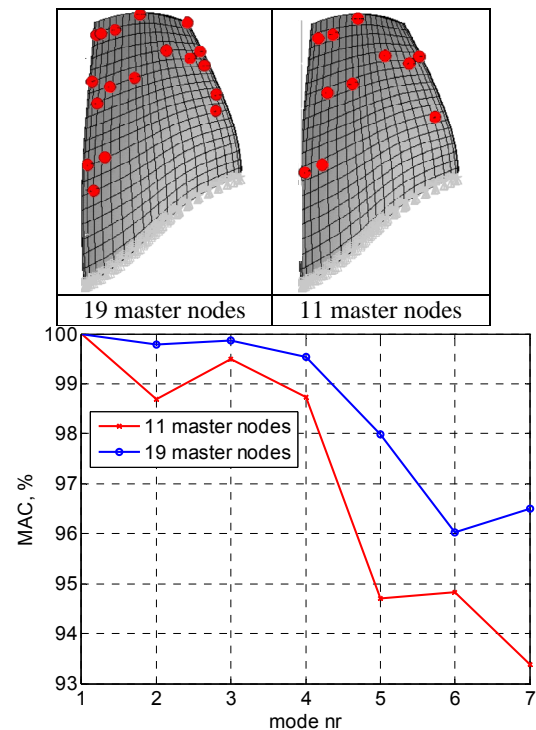


Figure 5-1: Different number of master nodes (above). MAC of reduced real modes when compared to the full real modes (below).

A first set of master nodes was selected and its accuracy with respect to the in-vacuo full mesh modes (Table 4-1) judged by the Modal Assurance Criteria (MAC). A MAC of 100 (equation 22) means a perfect match of the full mesh mode-shape with the resulting mode-shapes from the Guyan reduced mass and stiffness matrices. In the present study, an

appropriate set of master nodes should result in in-vacuo reduced mode-shapes with a MAC higher than 90 when compared to the full model. Figure 5-1 shows the different MAC numbers for the first 7 modes considering different sets of master nodes. Note increasing the master nodes implies a higher accuracy.

$$MAC = 100 \cdot \frac{(\phi_1^T \phi_2)^2}{(\phi_1^T \phi_1)(\phi_2^T \phi_2)} \quad (22)$$

A first set of 19 master nodes was selected.

5.2. Guyan-based Arbitrary Modes (GAMs)

Once the master nodes are selected, the arbitrary modes are produced in the following manner:

- 1) The structural system is Guyan reduced to one master node at a time
- 2) A displacement of $1e-3m$ is assigned to that master node in one Cartesian direction at a time, as in equation 23

$$\{q_x\} = \begin{bmatrix} 1 \cdot 10^{-3} \\ 0 \\ 0 \end{bmatrix} \quad (23)$$

- 3) A back-projection to the full model is done giving rise to the here called Guyan-based Arbitrary Mode (GAM) for that specific node and direction, as shown in equation 24.

$$\phi_{GAM,x} = [-K_{ss} [K_{sm}]^{-1} \{q_x\}] \quad (24)$$

In this case the number of master nodes is one and the slave nodes are the number of nodes in the full FE mesh minus the one master node. Following this procedure, a number of $master_nodes \times 3 dof$ Guyan-based Arbitrary Modes are obtained.

The resulting GAMs from displacing each master node in the axial direction are depicted in Figure 5-2. Arbitrary modes are also obtained from displacing the nodes in the radial (Y) and tangential (Z) direction.

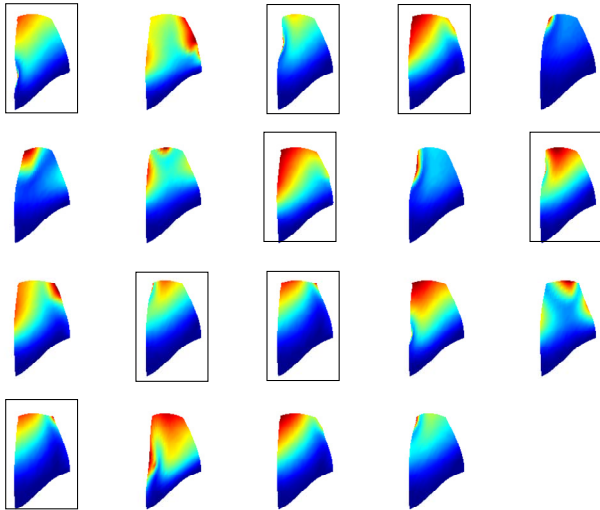


Figure 5-2: 19 GAMs from axial (X) displacement of master nodes. Absolute amplitudes. Eliminated modes highlighted

5.3. Filtering Redundant Modes

It is possible to visualize some redundant GAMs which could be eliminated from the set and thus reduce the number of CFD calculations. By performing a crossed MAC operation between the GAMs and eliminating those which give a MAC number above 80, it is possible to reduce the number of modes to 11 (a reduction of almost half). The eliminated modes are highlighted in Figure 5-2.

Also, considering that the radial displacement is not of great influence in the studied mode-shapes and furthermore considering that the vibration on this direction will not have a relevant influence on the unsteady aerodynamics, all the arbitrary modes rising from displacing the master node in the Y direction are eliminated.

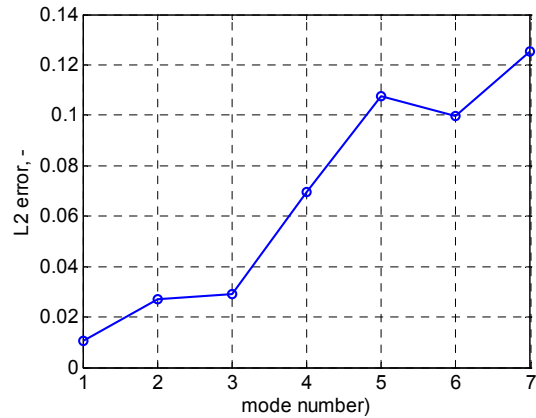


Figure 5-3: 19 Least Square error when fitting the 11 X and Z arbitrary modes to the real modes (above). Matched modes (below)

Finally, when combining all the GAMs linearly by a L^2 fit to the real first modes, the error obtained is increasing with increasing mode-shape, and reaches a maximum deviation of around 13% (Figure 5-3). This would in turn limit the precision of the final stability response considering only the mode-shape influences.

The final set of master nodes is reduced to 11 for consistency with the selected GAMs. The accuracy of the reduced real modes is still above a MAC of 90 for the first 7 modes (Figure 5-1). The final number of CFD calculations required is presented in the following table:

Frequency	Modes X	Modes Z	Total Modes	IBPA	Total
f_1	11	11	22	8	176
f_4	11	11	22	8	176
f_7	11	11	22	8	176
Total Number of CFD simulations					528

Table 5-1: Number of CFD unsteady calculations considering the GAMs

It must be noted that it is possible to utilize any other set of arbitrary modes under the consideration of being linearly independent and that when combined with L^2 approximation

could be accurately matched to any perturbed mode. The GAMs is one alternative here proposed, being consistent with a reduction technique applicable for mistuning analyses and that also allows parametric arbitrary modes generation. The selection of an arbitrary modes basis could then be optimized for a specific application.

6 RESULTS

In this section the stability analyses results from the GAMs using the MLS are presented. The results will be compared to the stability from the in-vacuo modes using the MLS general method. The influence of the frequency of oscillation of the GAMs is also discussed.

6.1. MLS Stability from In-vacuo Modes

The resulting stability considering the in-vacuo modes for the CFD calculations is presented in Figure 6-1. The different points at each mode represent the aerodynamic damping in terms of critical damping ratio at different nodal diameters (or inter blade phase angles). The negative aerodynamic damping means an unstable condition. Note that the mean value of the stability curves is set by the influence of the vibrating blade on itself and the amplitude of the curve by the influence of neighbor blades. Most of the mode-shapes considered experience a stable condition, with the exception of mode 1 which is marginally unstable. Even when the stability curve of mode 1 has the largest mean value, it also has the largest curve amplitude, and thus reaching an unstable condition. This is due to a large destabilizing effect of the neighbor blades. The aerodynamic coupling due to the aerodynamic forces can be observed in the change of frequency for the different inter blade phase angles, shown for mode 1 (zoom in Figure 6-1).

In order to compare the results obtained from the GAMs both the Stability Curve Amplitude (SCA), as well as the mean value of the curves will be considered.

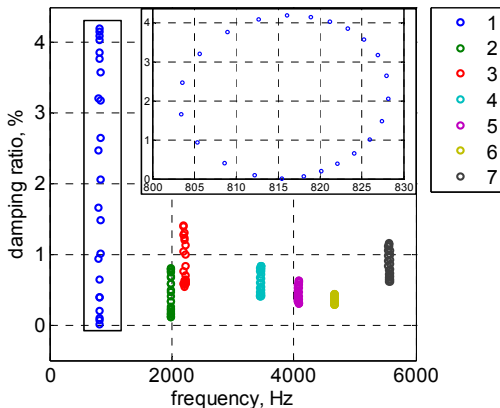


Figure 6-1: Aerodynamic damping from the first 7 real modes using the MLS general method. Zoom of mode 1

6.2. MLS GAMs at f_1

The stability obtained from the 22 harmonic forces from the GAMs considering the oscillation of all modes at f_1 is presented in Figure 6-2. Only the aerodynamic stiffness and damping matrices are calculated (equation 5 and 6).

In Figure 6-3 it is shown that there is a better approximation of both the SCA and the mean value for the 1st and 2nd

modes as compared to the higher modes. It is expected that the lower modes are matched in a better manner than the higher for two reasons: 1) the mode-shape fit for the lower modes is better than the larger modes (Figure 5-1) and 2) the frequency of oscillation is the lowest of the range. However, the deviation of the resulting stability of modes from 3 to 7 is much larger than what expected if only the difference in mode-shapes are accounted. This gives an indication of a great influence of the frequency on the unsteady forces.

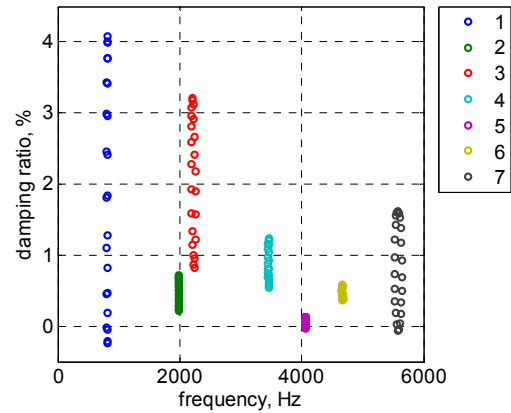


Figure 6-2: Stability from arbitrary modes oscillated at f_1

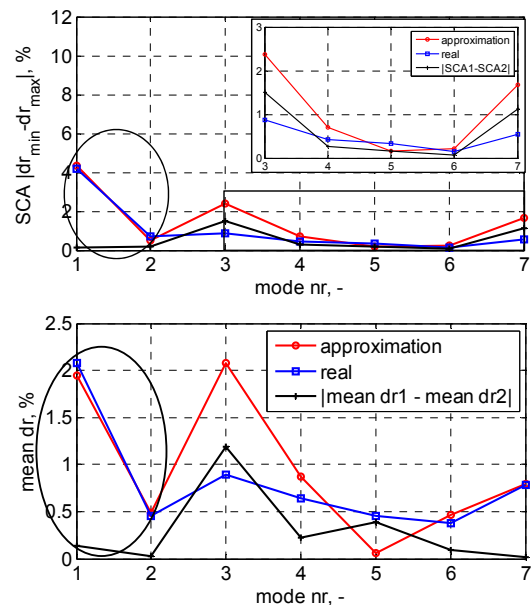


Figure 6-3: SCA (top) and Mean (bottom) and its differences with the real modes. Arbitrary modes oscillated at f_1

6.3. MLS GAMs at f_7

The stability considering the set of harmonic forces rising from the GAMs oscillation at f_7 has been calculated.

In this case both mean and SCA show a good approximation not only for mode 7 (the mode responding at f_7) but for modes 4 to 7 (Figure 6-4). From these results it seems clear that even when GAMs are matching well to the mode-shapes for the complete range, the major influence is then given by the frequency change. From modes 4 to 7 it could be seen that it behaves linearly.

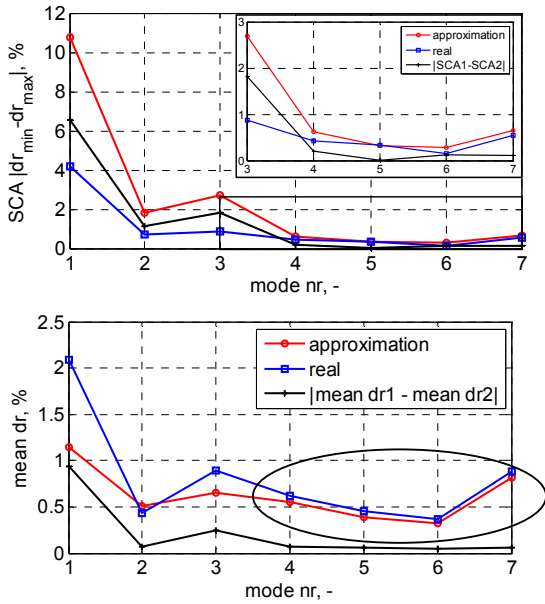


Figure 6-4: SCA (top) and Mean (bottom) and its differences with the real modes. Arbitrary modes oscillated at f_7

6.4. MLS GAMs at f_4

In order to explore if a better fit could be obtained by calculating a frequency in the middle of the range of interest, the GAMs have been calculated at the 4th mode frequency (3295Hz) and the stability of the 7 modes presented in Figure 6-5.

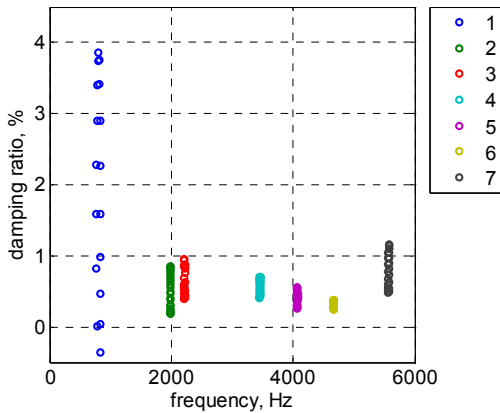


Figure 6-5: Stability from arbitrary modes oscillated at f_4

Both the stability curve amplitude and mean value present an acceptable accuracy from modes 2 to 7 (Figure 6-5). Mode 1 however is much better predicted by the GAMs oscillation at the mode 1 frequency.

For the higher modes, mode 3 shows the largest the deviation both in SCA and mean value. Considering the 1st, the 4th and 7th frequency of oscillation (Figure 6-3, Figure 6-4 and Figure 6-5), this mode has been the one with the major deviations.

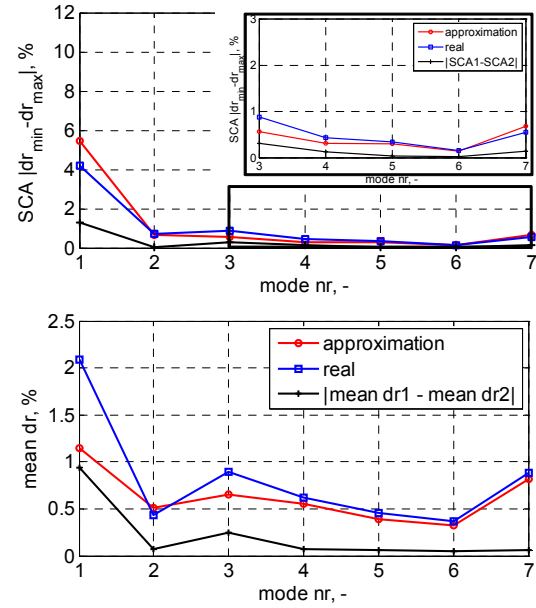


Figure 6-6: SCA (top) and Mean (bottom) and its differences with the real modes. Arbitrary modes oscillated at f_4

6.5. MLS GAMs Considering Two Ranges of Frequency

As seen from results in section 5.2 and 5.3, the oscillation of the GAMs at one frequency is not accurate for the complete range, but for rather limited ranges close to the oscillated frequency. Two smaller frequency ranges are studied, considering the middle frequency inside the range, in this case that of the 4th in-vacuo mode. One range oscillating the GAMs at f_1 and f_4 ; another considering the oscillation at f_4 and f_7 .

The aerodynamic mass matrix is included for these analyses. This allows fitting the real part of the harmonic forces from two frequencies. However the imaginary part, which is of major relevance in the stability outcome, can be only fitted to one frequency. In this case an average of the two possible aerodynamic damping matrices (one per frequency set of forces) of each influence coefficient is calculated (equation 18).

The differences obtained using the first range extreme frequencies f_1 and f_4 are presented in Figure 6-7, whereas the second range from f_4 and f_7 in Figure 6-8. It can be seen that using the second range of frequencies, the modes from 2 to 7 can be predicted with an acceptable accuracy, in both SCA and mean value. However, mode 1 still shows large deviations. When using the average of the damping from the 1st and 4th frequencies, the lower modes are not as accurately predicted as in the case when only the 1st frequency was used (Figure 6-3). This shows that a linear behavior of the imaginary forces in the lower range could only be considered for the frequencies between mode 1 and 2, and a different range would exist near the mode 3 and 4 frequencies. This can also explain that the 3rd mode had the largest deviations when using the 1st, 4th or 7th frequency.

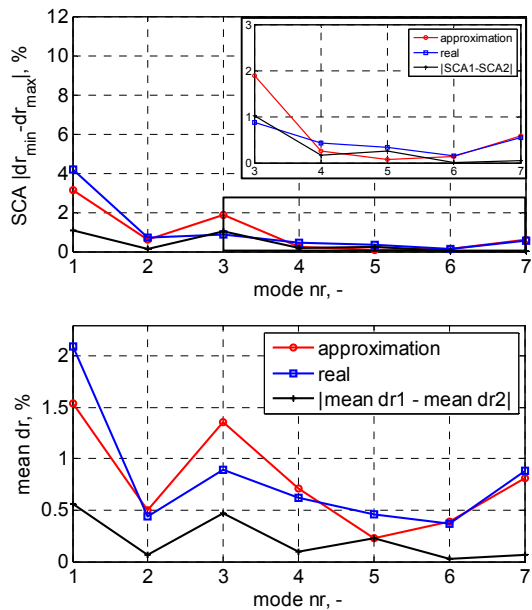


Figure 6-7: SCA (top) and Mean (bottom) and its differences with the real modes. Arbitrary modes oscillated at f_1 and f_4

On the other hand, the higher modes predicted in a similar manner by using the GAMs oscillated at f_4 , oscillated at f_7 , or using both results by including the aerodynamic mass contribution and the average in the damping matrices. This means that the stability in the frequency range of modes 4 to 7 could be predicted with half of the computations by only using the GAMs at the extreme oscillated frequency f_7 .

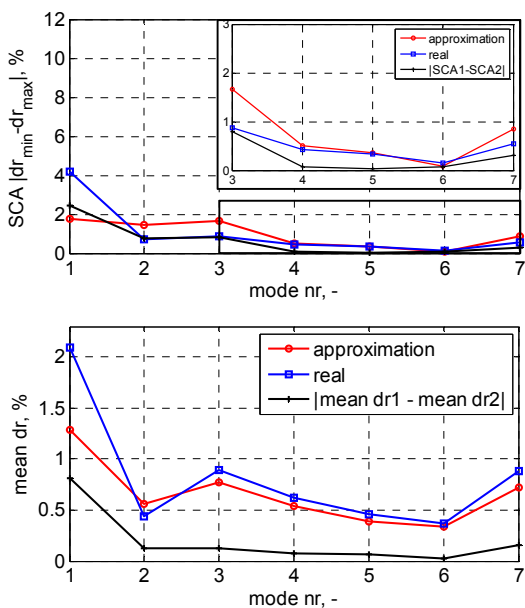


Figure 6-8: SCA (top) and Mean (bottom) and its differences with the real modes. Arbitrary modes oscillated at f_4 and f_7

Looking to the results, it seems clear that the most efficient procedure is to calculate the set of forces from the oscillation at a frequency in the middle of the range of interest rather than calculating two extreme frequency sets and calculating the average. However, having two frequencies allows for a better fit of the real contributions

(aerodynamic mass and stiffness) in a wider range and the major limitation is due to the linear fit of the aerodynamic damping. Determination of the boundaries of the linear frequency behavior range is discussed in the following section.

7 DISCUSSIONS

In this section a discussion regarding the frequency influence is given as well as the relation of the different GAMs and their resulting unsteady forces. With this it is aimed at understanding the physical behavior of the flow and how this understanding could be used for a general application of the method highlighting what are important considerations.

7.1. Frequency Influence

With the purpose of understanding the influence of a large frequency variation on the aerodynamic damping, further CFD calculations are performed for a selected mode at different inter blade phase angles. The mode selected is the 1st real mode since it has shown to have the largest unsteady amplitudes (high SCA and mean value) and its change with frequency could be better observed. Mode 1 was then oscillated at the 7 different frequencies of the in-vacuo modes (Table 4-1). The influence coefficient generalized forces (i.e. the projection of the harmonic forces onto the 1st mode) are shown in Figure 7-1. The different curves represent the influences of the different blades on the overall stability, being blade 0 the influence of the oscillating blade on itself.

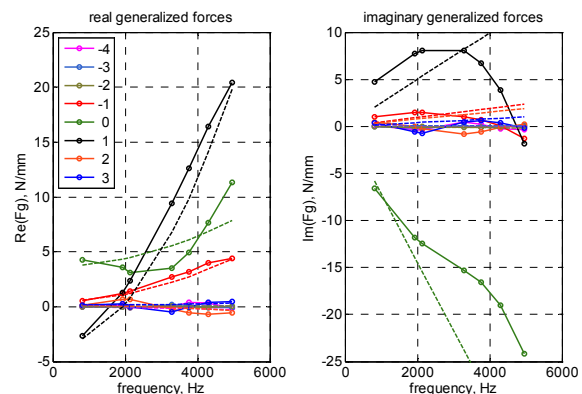


Figure 7-1: Generalized real (left) and imaginary (right) forces of the 1st mode at different frequencies. Influence Coefficient domain; MLS GAMs frequency fit in dashed lines

In this case the negative value of the generalized force means a stabilizing condition. When looking at the imaginary contribution, which is the most relevant considering the stability, it is observed that as expected the blade influence on itself (blade 0) has a stabilizing character. It becomes even more stable with increasing frequency and follows an approximated linear pattern consistent with the method here applied. This will in turn have the major influence on the mean stability curve value which can then be well predicted. The second largest influence is that of blade +1, in which case the influences are becoming more destabilizing in the first range of frequencies and then become more stabilizing after 4th frequency. This trend of

blade +1 conditions the accuracy of the predictions, since it is clearly non-linear. The imaginary influences of the other blades are much lower for the complete range of frequencies studied. A similar relation was observed by all the GAMs when observing the same trends of the 3 frequency points calculated.

The real part of the forces is of interest when looking at the aerodynamic coupling strength, which can be observed in a change in frequency of a responding mode, different to that of the in-vacuo frequency. In this case blade 0 and the adjacent neighbor blades are the most influential. Here, blades -1 and +1 show a linear behavior in the complete range and blade 0 only shows this after the 4th frequency. This would mean that for both real and imaginary part a linear trend could be fitted from the 1st to the 2nd frequency and a second from the 4th to 7th, consistent with the behavior of the MLS arbitrary modes approach calculated at the extreme frequencies (Figure 6-3 and Figure 6-4). A third frequency range would then be needed around the 2nd to the 4th mode frequency.

The above indicates that a first frequency study could be performed, considering only one mode at different frequencies of interest. This allows determining what the possible linear ranges boundaries are and the frequency for the oscillation of the GAMs modes could be selected in the middle of those boundaries

On the other hand, having two different frequencies can be used to fit the real contributions quite accurately the complete range by including the aerodynamic mass term into the equation. In Figure 7-1 (left) the dashed lines indicate the fitted aerodynamic forces from the GAMs aerodynamic mass and stiffness matrices when the system responds to mode 1. The prediction of the imaginary forces is however limited by the conditions that 1) at zero frequency the forces should be zero and 2) its increment depends on a single damping constant. Figure 7-1 (right) shows then the fit by considering the average of the extreme frequencies aerodynamic damping matrices.

Even when the MLS application using the GAMs requires a larger number of CFD computations as compared to using the mode-shape of interest directly, the method allows for larger generality: this is it can be applied to a system that could respond to perturbed mode-shapes, as well as allowing differences in frequency to the in-vacuo one due to different sources of perturbations (e.g. mistuning or aerodynamic coupling). On the other hand, it opens up for its application on forced response analyses, where the aerodynamic damping is then adjusted in the model to any responding frequency in a common numerical frequency sweep.

7.2. GAMs Influence on the Unsteady Response

In order to study what is the influence of mode-shapes in the unsteady response, the imaginary generalized forces of all the GAMs have been calculated by projecting the mode-shapes onto the influence coefficient harmonic forces.

In Figure 7-2 it is shown that for all the considered modes, the influence of blade 0 and the blade +1 are the largest, as seen for the mode shape 1. This means that all possible

modes produced from the linear superposition of the GAMs will also have this behavior.

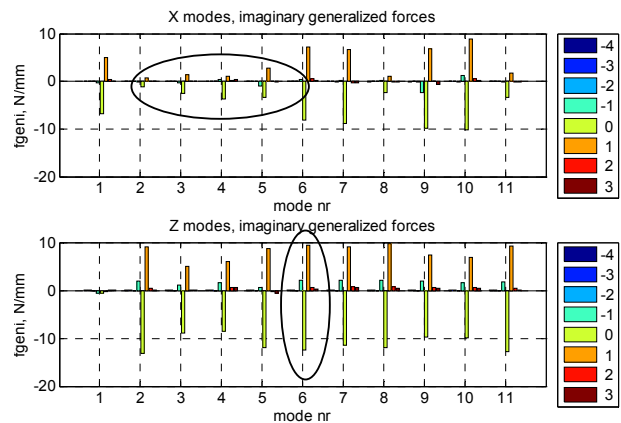


Figure 7-2: Influence Coefficient generalized forces of all the GAMs at f_1

It can also be observed that the GAMs obtained from displacing the nodes in the tangential direction have a slightly larger unsteadiness effect than the ones from displacing the master nodes in the axial direction. It is important to highlight that both X and Z modes have a motion in all the 3 directions, but the major contributions are on the corresponding direction at which it was projected from. Figure 7-2 also tells which GAMs are the least influential, such as modes 2-5 of the X modes.

The blade 0 imaginary pressure coefficients of these modes are depicted in Figure 7-3. The low resulting generalized forces occur when the regions of large unsteadiness are not located where substantial motion exists. This results in a very low aerodynamic damping for those modes. The opposite happens in modes with a high generalized force, as for example mode 6 from the set of Z GAMs. This mode has a large area of displacement from mid-span towards the tip and thus matching with the unsteadiness of the flow in both pressure and suction side.

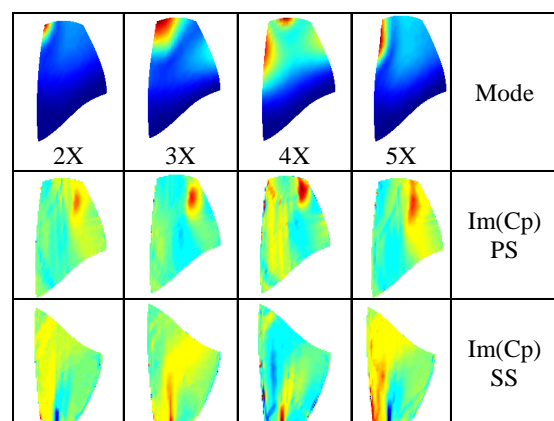


Figure 7-3: Imaginary pressure coefficient for the X modes 2-5. Influence of blade 0 on itself

Also, the originated unsteadiness from this mode is of larger amplitude and covers most of the span of the blade. The in-

vacuo mode 1 is also having this kind of shape and thus it also experiences a large SCA and mean value.

An important observation is that major unsteadiness occurs in the tip where shocks have the major influence. This behavior holds for most of the GAMs and for both influences of blade 0 and +1 (Figure 7-5 and Figure 7-6).

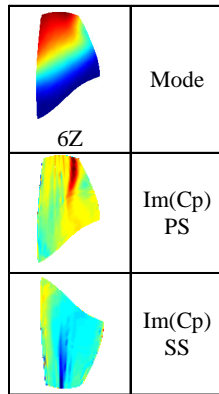


Figure 7-4: Imaginary pressure coefficient for the mode 6 Z. Influence of blade 0

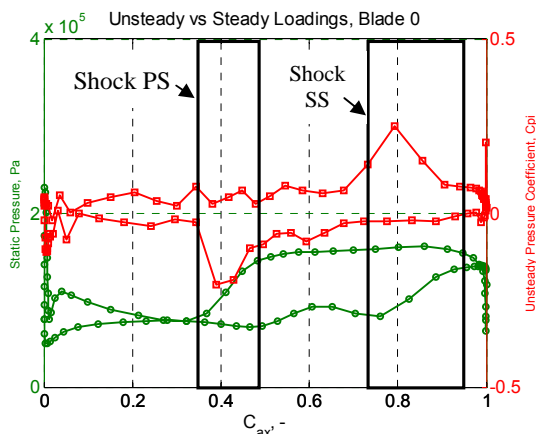


Figure 7-5: Static pressure vs. imaginary Cp loading at 90% span. GAM 6Z Influence of blade 0. Shock regions highlighted

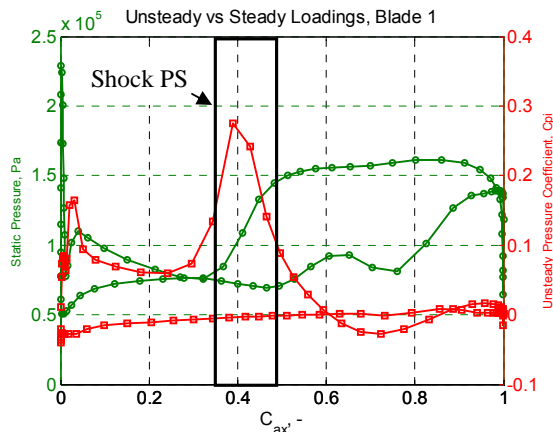


Figure 7-6: Steady vs. unsteady loading at 90% span. GAM 6Z Influence of blade 1. Shock regions highlighted

This means that knowing the expected locations of high unsteadiness from the steady state loading, then the GAMs

to include could further be filtered out considering which will be most influential for the stability analysis and thus reducing the number of modes for calculation using CFD.

However, there are cases in which determining the aerodynamic damping of low damping modes is of interest, such as when predicting how much mechanical damping is then required maintaining low amplitude levels in forced response analyses. In such cases, it is then important to keep the low aerodynamically damped modes in the model.

8 SUMMARY AND CONCLUSION

A new method for determination of the aeroelastic behavior of perturbed modes based on Least Square approximations has been presented. The method includes the aeroelastic properties of the system in a wide general manner such as to allow responding mode-shapes different to the tuned-in-vacuo ones. This approach requires the unsteady CFD calculation of a larger number of modes as in typical single mode families approaches, but allows the possibility of fitting to mode-shapes that can be perturbed due to mistuning, highly aerodynamically loaded blades, coating damping and other source of mode perturbation. The method is consistent with a reduction technique that can be used for high strength mistuning analyses having a model size that permits probabilistic analyses. It has been shown here that decreasing the number of master nodes to 11 (0.5% of the full model) the first 7 real mode-shapes could be matched with an accuracy of 93% for the 7th mode up to 99.9% for the 1st mode. The unsteady forces are thus obtained from a limited number of arbitrary modes (GAMs) that are also consistent with the reduction applied. The application of the method on a highly loaded transonic rotor blade shows that including the aerodynamic forces calculated at a single frequency would approximate best to the mode-shapes responding to that frequency but also to a range of neighbor modes if the main influences of the imaginary forces behave linearly with the frequency in that range. However, the real forces can be fitted accurately by including the aerodynamic mass contribution from the two extreme frequencies in the range. It has been observed that the unsteady forces relation with the frequency tends to be similar for different mode-shapes and thus a first frequency study with a specific mode can be carried out for determining the frequency linear behavior where the method can be applied. In transonic compressors, the location of shocks is a good indicator where major unsteadiness due to blade motion is expected and thus this can also be a good indicator of which arbitrary modes would be influential and worth to perform the CFD calculations. The accuracy of the prediction will be limited on how well the GAMs match the responding mode. In the present case, the 1st real mode could be predicted with an accuracy of 97% for mean of the stability curve and 90% for the SCA which corresponded to a L² mode-shape GAMs match of 98%. Structural coupling effects can be accounted using the proposed method, by including the couplings of the disk in the structural matrices. The reduced model implementation thus allows for complete aerodynamically and structurally coupled mistuning analyses, being this one of the strengths of the method which foundation is assessed in this paper.

9 ACKNOWLEDGEMENTS

The research has been funded by the Swedish Energy Agency, Siemens Industrial Turbomachinery AB and Volvo Aero Corporation through the Swedish research program TURBO POWER, the support of which is gratefully acknowledged. The generous support of the Swedish Defense Procurement Agency (FMV) to the development and research in compressors is also recognized.

10 REFERENCES

[1] Crawley E., "Aeroelastic Formulation for Tuned and Mistuned Rotors". AGARD Manual on Aeroelasticity in Axial-Flow Turbomachines. Vol 2. Structural Dynamics and Aeroelasticity.

[2] Kielb R. E., Hall K.C., Miyakozawa T., 2007, "Flutter of Mistuned Bladed Disks and Blisks with Aerodynamic and FMM Structural Coupling". Proceedings of ASME Turbo Expo, GT2007-27503.

[3] Miyakozawa T., Kielb R., Hall K., 2008, "The Effects of Aerodynamic Asymmetric Perturbations on Forced Response Bladed Disks". Proceedings of Turbo Expo 2008. GT2008-50719.

[4] Martel C., Corral R., Llorens J., 2008, "Stability Increase of Aerodynamically Unstable Rotors Using Intentional Mistuning". ASME Journal of Turbomachinery, Vol. 130, 011006.

[5] Martel C., Corral R., 2009, "Asymptotic Description of Maximum Mistuning Amplification of Bladed Disk Forced Response". ASME J. Eng. Gas Turbines Power, Vol. 131, 022506.

[6] Gerolymos G. A., 1993, "Coupled Three-Dimensional Aeroelastic Stability Analysis of Bladed Disks". ASME Journal of Turbomachinery. Vol. 115, pp. 791-799, October 1993.

[7] Mårtensson H., Gunnsteinsson S., Vogt D., 2008, "Aeroelastic Properties of Closely Spaced Modes for a Highly Loaded Transonic Fan". Proceedings of ASME Turbo Expo 2008. GT2008-51046.

[8] Clark S., Kielb R., Hall K., 2009, "The Effect of Mass Ratio, Frequency Separation, and Solidity on Multi-Mode Fan Flutter". Proceedings of the 12th International Symposium on Unsteady Aerodynamics, Aeroacoustics & Aeroelasticity of Turbomachines. Imperial College London, ISUAAAT 12. I12-S3-2.

[9] Mayorca M., Vogt D., Mårtensson H., Fransson T., 2010, "A New Reduced Order Modeling for Stability and Forced Response Analysis of Aero-Coupled Blades Considering Various Mode Families". Proceeding of ASME Turbo Expo 2010. GT2010-22745.

[10] Glodic N., Bartelt M., Vogt D., Fransson T., 2009 "Aeroelastic Properties of Combined Mode Shapes in an Oscillating LPT Cascade". Proceedings of the 12th International Symposium on Unsteady Aerodynamics, Aeronautics & Aeroelasticity in Turbomachines. Imperial College London, ISUAAAT 12. I12-S8-2.

[11] Mårtensson H., 2005. "A Method for Deriving an Aeroelastic Model from Harmonic CFD results". ISABE-2005-1255

[12] Guyan R., 1965, "Reduction Stiffness and Mass Matrices", AIAA Journal, 3(2): 380.

[13] Mårtensson H., Burman J., Johansson U., 2007, "Design of the High Pressure Ratio Transonic 1 1/2 Stage Fan Demonstrator Hulda". ASME Paper No. 2007-GT-27793

[14] Eriksson, L. E., 1993, "A Third Order Accurate Upwind-based Finite-Volume Scheme for Unsteady Compressible Viscous Flow". Technical Report, VAC Report 9370-154, Volvo Aero Corporation.

[15] Mayorca M., Vogt D., Mårtensson H., Fransson T., 2009. "Numerical Tool for Prediction of Aeromechanical Phenomena in Gas Turbines". ISABE-2009-1250.